Int. J. Heat Mass Transfer. Vol. 36, No. 4, pp. 949–959, 1993
Printed in Great Britain

0017–9310/93 $6.00 + 0.00

Heat transfer past particles entrained in an oscillating flow with and without a steady velocity

MAN YEONG HA,† SAVASH YAVUZKURT‡ and KYUNG CHUN KIM†

†Department of Mechanical and Production Engineering, The Pusan National University, 30 Jangjeon-Dong, Kumjung Ku, Pusan 609-735, Korea

‡Department of Mechanical Engineering, The Pennsylvania State University, University Park, PA 16802, U.S.A.

(*Received* 4 *January* 1991 *and in final form* 28 *April* 1992)

Abstract—In order to investigate the heat transfer past particles entrained in an oscillating flow with and without a steady velocity, the two-dimensional, unsteady conservation equations of mass, momentum and energy for laminar flow in the gas phase are solved numerically in spherical coordinates. The particle momentum equation is also solved simultaneously with the gas phase equations in order to consider the effect of the particle entrainment on the heat transfer past particles. The numerical solution gives the particle velocity variation as well as the gas phase velocity and temperature distribution as a function of time. The local and space-averaged Nusselt number with particle entrainment is compared with that without particle entrainment. In the case of an oscillating flow with a steady velocity, the values of the space-averaged Nusselt number with particle entrainment are lower than those without particle entrainment at frequencies of 50 and 2000 Hz, since the moving particle is entrained in the steady velocity. In the case of an oscillating flow without a steady velocity, the space-averaged Nusselt number with entrainment at a frequency of 50 Hz is slightly lower than that without particle entrainment, with a phase lag. At 2000 Hz, the space-averaged Nusselt number with and without particle entrainment is almost the same, due to very small particle entrainment.

INTRODUCTION

THE EFFECT of an oscillating flow field with and without a steady velocity component on heat and mass transfer from single spherical particles and droplets has been a topic of investigation since the late 1930s [1]. Some examples of these theoretical and experimental studies can be found in refs. [2–7]. These publications report an increase, decrease or unnoticeable change in heat and mass transfer, depending on the frequency and the magnitude of the steady and oscillating flow. Zinn *et al.* [8] and Faeser [9] indicated the positive effects of high intensity acoustics on coal combustion by using acoustic drivers or pulsed combustion. Koopmann *et al.* [10] investigated the effects of high intensity acoustic fields on the rate of combustion of coal–water slurry fuel in the sonic combustor. Yavuzkurt *et al.* [11, 12] calculated a decrease of 15.7 and 12.1%, respectively, in the char burn-out length for a sound pressure level of 160 dB and at a frequency of 2000 Hz compared to the case with no sound for the combustion of 100 μm pulverized coal or coal–water slurry fuels.

The previous studies are generally concentrated on experimental and theoretical studies showing the effects of oscillating flow field on heat and mass transfer and combustion past particles, in which it is usually assumed that the particle is stationary relative to its gaseous environment. Thus, the particle momentum equation is not included with the constant slip velocity between the particle and the bulk gas stream. However, in the initial stages of combustion of pulverized coal or coal–water slurry droplets, there exists a steady slip velocity, U_0. This steady slip velocity decreases during combustion since coal particles or particle agglomerates become entrained in the main gas flow. During the later stages of pulverized coal or coal–water slurry fuel combustion, the slip velocity between the entrained particles and the gas is quite low for a significant period of time, leading to low heat and mass transfer to and from the particles. For this situation, the particle momentum equation should be solved simultaneously with gas phase equations and the slip velocity continuously changes depending on the particle trajectories.

In order to investigate heat transfer past particles entrained in an oscillating flow with a steady velocity component, an oscillating flow, $U_1 \cos(2\pi ft)$, induced by the high intensity acoustic fields is superposed on the mean steady flow, U_0, in the present study. The two-dimensional, unsteady conservation of mass, momentum and energy equations for a laminar flow past particles in spherical coordinates was solved simultaneously with the particle momentum

NOMENCLATURE

dB	decibel
D	diameter
f	frequency
h_θ	local heat transfer coefficient
i	static enthalpy
k	thermal conductivity
m_p	particle mass
Nu	Nusselt number
P	pressure
Pr	Prandtl number
r	radial position
R	radius of particle
R	gas constant
Re_0	steady Reynolds number, $(U_0 D/\mu)$
Re_1	acoustic Reynolds number, $(U_1 D/\mu)$
S	Strouhal number, (fD/U_1)
S_ϕ	source term for general variable ϕ
t	time
T	temperature
T	period
u_r	radial velocity
u_θ	axial velocity
U_0	steady slip velocity
U_1	acoustic peak velocity
v_g	gas velocity
v_p	particle velocity.

Greek symbols

β	angular direction defined in the streamwise direction
γ	specific heat
Γ_ϕ	diffusivity for general variable ϕ
ε_ϕ	convergence criteria
ε	velocity ratio
θ	angular direction
μ	viscosity
ρ_g	gas density
τ	dimensionless time (ft or t/T)
τ_s	quasi-steady dimensionless time
ϕ	general variable given in equation (1)
ω	angular frequency.

Subscripts

g	gas
new	new values
old	old values
p	particle
r	radial
s	space-averaged
s	separation
0	steady
0	initial
1	acoustic
θ	angular
ϕ	dependent variables
∞	infinity.

equation. The results obtained considering particle entrainment are compared with those without entrainment.

GOVERNING EQUATIONS AND BOUNDARY CONDITIONS

The hydrodynamic and thermal characteristics of an oscillating flow created by an acoustic field over a single particle are studied by solving the unsteady and two-dimensional axisymmetric conservation equations for constant property, laminar flow with the following common form [13]:

$$\frac{\partial}{\partial t}(\rho\phi)+\frac{1}{r^2}\frac{\partial}{\partial r}(r^2\rho u_r\phi)+\frac{1}{r\sin\theta}\frac{\partial}{\partial\theta}(\sin\theta\,\rho u_\theta\phi)$$
$$=\frac{1}{r^2}\frac{\partial}{\partial r}\left(\Gamma_\phi r^2\frac{\partial\phi}{\partial r}\right)+\frac{1}{r^2\sin\theta}\frac{\partial}{\partial\theta}\left(\Gamma_\phi\sin\theta\frac{\partial\phi}{\partial\theta}\right)+S_\phi. \quad (1)$$

The flow field and the particle geometry with some nomenclature are shown in Fig. 1. In the conservation of momentum equation, $\phi = u_r, u_\theta$ represents the velocities in the radial r and axial θ directions, respectively. In the energy equation $\phi = i$ is the static enthalpy. The source terms S_ϕ in equation (1) are given in Table 1. The quantities are allowed to vary in the radial (r) and axial (θ) directions whereas a circumferential symmetry is assumed around an axis which passes through the center of the particle and is parallel to the flow direction.

The governing equation (1) has the following initial and boundary conditions.

Initial conditions ($t = 0$):

$$\phi = \phi_0. \quad (2)$$

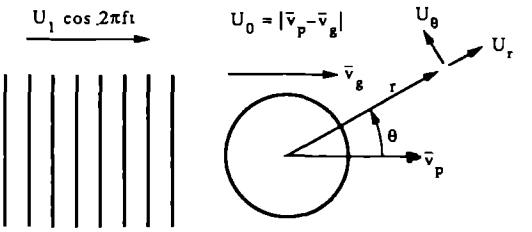

FIG. 1. Schematic diagram showing the geometry and some of the nomenclature used to simulate heat transfer past a spherical particle entrained in an oscillating flow.

Table 1. Source terms in S_ϕ in equation (1)

ϕ	Γ_ϕ	S_ϕ
1	0	0
u_r	μ	$-\frac{\partial p}{\partial r}+\frac{1}{r^2}\frac{\partial}{\partial r}\left(\mu r^2\frac{\partial u_r}{\partial r}\right)+\frac{1}{r\sin\theta}\frac{\partial}{\partial\theta}\left(\mu\sin\theta\frac{\partial u_\theta}{\partial r}\right)$ $-\frac{1}{r^2\sin\theta}\frac{\partial}{\partial\theta}(\mu\sin\theta u_\theta)-\frac{2\mu}{r^2}\frac{\partial u_\theta}{\partial\theta}-4\mu\frac{u_r}{r^2}$ $-2\mu\frac{u_\theta\cot\theta}{r^2}+\rho\frac{u_\theta}{r^2}$
u_θ	μ	$-\frac{1}{r}\frac{\partial p}{\partial\theta}+\frac{1}{r^2}\frac{\partial}{\partial r}\left(\mu r^2\frac{\partial u_\theta}{\partial r}\right)+\frac{1}{r^2\sin\theta}\frac{\partial}{\partial\theta}\left(\mu\sin\theta\frac{\partial u_\theta}{\partial\theta}\right)$ $+\frac{2}{r\sin\theta}\frac{\partial}{\partial\theta}\left(\mu\sin\theta\frac{u_r}{r}\right)+\frac{\mu}{r}\frac{\partial u_\theta}{\partial r}+\frac{\mu}{r^2}\frac{\partial u_r}{\partial\theta}-\mu\frac{u_\theta}{r^2}$ $-2\mu\frac{u_r\cot\theta}{r^2}-2\mu\frac{u_\theta\cot^2\theta}{r^2}-\frac{1}{r^2}\frac{\partial}{\partial r}(\mu r u_\theta)-\rho\frac{u_r u_\theta}{r^2}$
i	k/c_p	0

Boundary conditions ($t > 0$):

$$\frac{\partial\phi}{\partial\theta}=0, \quad \text{at} \quad \theta=0 \quad \text{and} \quad \pi \text{ (symmetry conditions)} \tag{3}$$

$$\phi=\phi_p, \quad \text{at} \quad r=R \tag{4}$$

and as $r\to\infty$

$$\begin{aligned} u_\theta &= -[U_0+U_1\cos(2\pi ft)]\sin\theta \\ u_r &= [U_0+U_1\cos(2\pi ft)]\cos\theta \\ i &= i_\infty . \end{aligned} \tag{5}$$

In equations (4) and (5), ϕ_p represents the value of the dependent variable ϕ at the particle surface, U_0 is the steady component of the flow velocity with respect to the particles and U_1 is the peak value of the acoustic velocity as defined by:

$$U_1=\frac{\sqrt{2}\,10^{(L_p-94)/20}}{\rho_g(\gamma RT_g)^{0.5}} \tag{6}$$

where L_p represents the sound pressure level with the unit of dB. The present study considers only the case of a longitudinal acoustic field. Thus the steady velocity, U_0, and acoustic velocity, $U_1\cos(2\pi ft)$, are co-linear. The velocities u_{rp} and $u_{\theta p}$ in equation (4) are zero. The static enthalpy i_p is a constant value determined by a specified particle temperature.

In the presence of oscillating flow fields, the particle is at least partially entrained (but with a phase lag) in an oscillating flow field. At high frequency, the magnitude of this entrainment is small. However, at low frequency, the particle is substantially entrained in the surrounding gas fields. In the present calculations, the particle momentum equation is included in order to consider particle entrainment.

The particle momentum equation is expressed as [10]:

$$m_p\frac{dv_p}{dt}=\Gamma_d(v_g-v_p) \tag{7}$$

where

$$\Gamma_d=4\pi R^2\rho C_d|v_g-v_p|/2 \tag{8}$$

$$C_d=(24/Re)(1+0.15Re^{0.687}) \tag{9}$$

$$Re=|v_g-v_p|D/\mu \tag{10}$$

where v_p in equation (7) represents the particle velocity and v_g represents $U_0+U_1\cos(2\pi ft)$ for the oscillating flow due to the acoustic field with a steady velocity component.

METHOD OF SOLUTION

The particle momentum conservation equation (7) with an unknown v_p are coupled to the gas phase conservation equations (1) with four unknowns (u_r, u_θ, p, i). Thus, coupled, nonlinear, unsteady and two-dimensional conservation equations with a total of five unknowns need to be solved simultaneously.

If the coordinate system is fixed in the ground, the grid system in the solution domain should move with the particle in order to consider particle entrainment. This is very difficult to implement numerically. In order to solve this problem, the coordinate system is fixed on the entrained particle. This results in the following extra source terms of the u_θ and u_r since the coordinate system is noninertial:

$$S_{u_\theta}=S_{u_\theta}+\rho\frac{dv_p}{dt}\sin\theta \tag{11}$$

$$S_{u_r}=S_{u_r}-\rho\frac{dv_p}{dt}\cos\theta. \tag{12}$$

The boundary conditions for u_θ and u_r as $r\to\infty$ are also adjusted as follows:

$$u_\theta=-[U_0+U_1\cos(2\pi ft)-v_p]\sin\theta \tag{13}$$

$$u_r=[U_0+U_1\cos(2\pi ft)-v_p]\cos\theta. \tag{14}$$

The gas phase equations are first solved using the same SIMPLEC procedure of Doormaal and Raithby [14]. Using this solution, the particle conservation equations are solved to yield the updated source terms for the gas phase, since the particle is entrained in the surrounding gas fields. The gas phase equations are solved again using these updated source terms, establishing the new solution for the gas field. This iterative procedure is repeated until the convergence criteria ε_ϕ for the gas phase equations given by equation (15) are satisfied.

$$\varepsilon_\phi=\sum\left|\frac{\phi_{new}-\phi_{old}}{\phi_{new}}\right| \tag{15}$$

where ϕ_{old} represents the values of the previous iteration and ϕ_{new} the updated values from the present iteration for u_r, u_θ and i.

The numerical solutions of the gas phase equation

(1) and particle momentum equation (7) give the velocity and temperature fields for oscillating flow over a spherical particle as a function of time, with a particle velocity history. From the calculated temperature distribution, the local Nusselt number, Nu_θ, is calculated as

$$Nu_\theta = \frac{h_\theta D}{k} = \frac{D}{(T_p - T_\infty)} \left.\frac{\partial T}{\partial r}\right|_{r=R}. \quad (16)$$

Integrating the local Nusselt number in the axial direction, the space-averaged Nusselt number, Nu_s, is obtained. This is given by the following equation:

$$Nu_s = \frac{1}{\pi}\int_0^\pi Nu_\theta \, d\theta. \quad (17)$$

RESULTS AND DISCUSSION

In the present simulation of heat transfer to and from a single spherical particle, the fluid is air with a free stream temperature of 20°C. The particle temperature is taken to be 40°C. The thermophysical properties such as viscosity, thermal conductivity, specific heat, etc. are calculated at a film variation between 20 and 40°C. The particle diameter is fixed at 100 μm in order to consider heat and mass transfer to and from small spherical particles such as pulverized coal particles and coal–water slurry droplets. The numerical solution domain is chosen to be 20 times the particle diameter with 30 grid points in the θ, and 50 in the r direction. The steady velocity (U_0), the amplitude of the oscillating velocity (U_1) and the frequency (f) of the applied acoustic field are varied in order to obtain the values of the Nusselt numbers for different steady and acoustic Reynolds and Strouhal numbers. One period or cycle is divided into 40 uniform time intervals, so that $\delta t = 1/40f$ is used as a numerical time step. A value of 0.005 is used for ε_ϕ in equation (15) as a convergence criterion in the present simulation.

Figure 2 shows a comparison of the separation angle β_s (measured in degrees) from the front stagnation point, obtained from the present simulation, with the approximate correlation given by Clift *et al.* [15], obtained from the numerical and experimental results for the steady Reynolds number range of 10–400 (without a superposed oscillating velocity, $Re_1 = 0$). As shown in Fig. 2, the present results for the separation angle β_s represent well the correlation given by Clift *et al.* [15]. Figure 2 also shows a comparison of the Nusselt number obtained from the present simulation with previously published numerical and experimental results in refs. [3, 16–19] for the steady Reynolds number range of 10–100 (without a superposed oscillating velocity, $Re_1 = 0$). The present results agree well with the numerical results given by Sayegh and Gauvin [16]. Sayegh and Gauvin indicated excellent agreement between previous numerical results and their calculations. They used a 30 × 40 grid

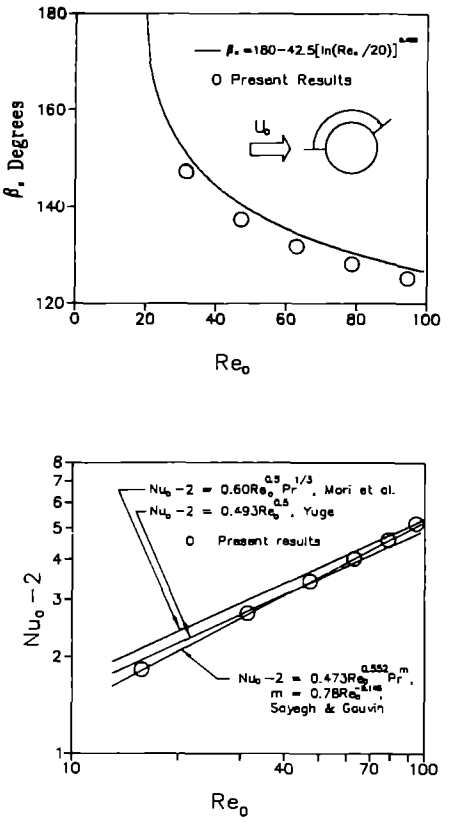

FIG. 2. Comparisons of separation angle (β_s) and Nusselt number ($Nu_\theta - 2$) obtained from the present simulation, with previous numerical and experimental results.

in the θ and r directions, respectively. However, the present results are somewhat higher than Yuge's correlation [17] obtained from experimental data for Reynolds numbers around 100 and are somewhat lower for Reynolds numbers around 10. This is also true for the numerical results of Sayegh and Gauvin [16] and Wong *et al.* [18]. For the case of an oscillating flow with and without a steady velocity component under the assumption that the particle is not entrained but is stationary in the presence of an oscillating flow, the results for space- and time-averaged Nusselt number using a present code represent well the correlations obtained from the quasi-steady analysis for a frequency of 50 Hz, as shown by Ha [7]. Under the assumptions of no particle entrainment, the particle momentum equation (7) is not considered ($v_p = 0$). These comparisons show that the present code is adequate for predicting the steady and oscillating flow field and heat transfer for a spherical particle.

Oscillating flow with a steady velocity

Figure 3 shows the oscillating flow U, the entrained particle velocity v_p and the relative velocity ($U - v_p$) at 50 Hz, in order to investigate heat transfer past particles entrained in an oscillating flow with a steady velocity component. The applied acoustic field U

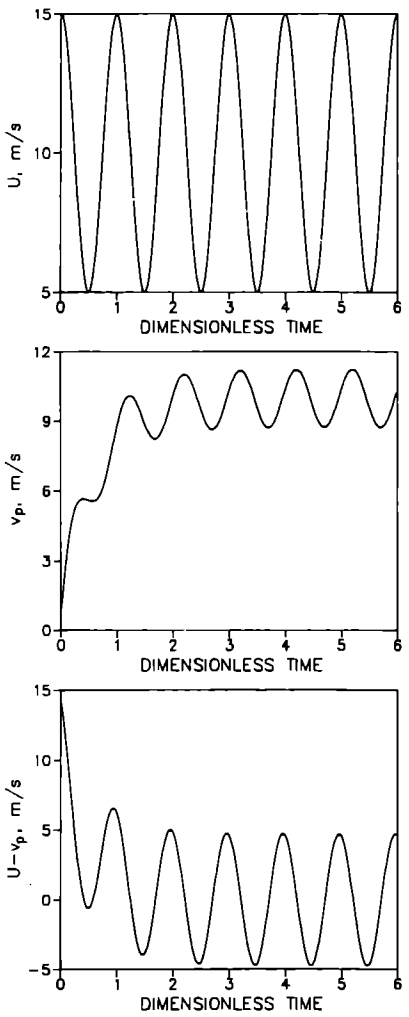

FIG. 3. Oscillating flow U, the entrained particle velocity v_p and the relative velocity $(U-v_p)$ as a function of dimensionless time: $Re_0 = 62.9$, $Re_1 = 31.5$, $S = 0.0005$ ($f = 50$ Hz).

oscillates with an amplitude of $U_1 = 5$ m s^{-1} around a steady velocity of $U_0 = 10$ m s^{-1}. During the initial and transient period, the particle velocity increases to about 10 m s^{-1} due to a major contribution of a steady velocity U_0, meaning that the particle is almost entrained to the steady flow. After a steady periodic state is reached, meaning that the particle velocity over a cycle is the same as the value obtained in the following cycles, the particle velocity oscillates with an amplitude of about 1.24 m s^{-1} around a steady velocity of 10 m s^{-1}. The phase lag between the gas and particle velocity is about 78° ($\tau = 0.2$). Thus the relative velocity $(U-v_p)$ has an initial decrease due to particle entrainment, followed by the steady periodic oscillation with an amplitude of about 4.7 m s^{-1}, as shown in Fig. 3. The phase lag between the gas and relative velocity is about 18° ($\tau = 0.05$). Even though the particle oscillates with an amplitude of 1.24 m s^{-1} around a steady velocity of 10 m s^{-1}, the amplitude of relative velocity still has a value of 4.7 m s^{-1} slightly lower than the oscillating velocity U_1 ($=5$ m s^{-1}), due to the phase difference. Thus, the boundary layer formed over the particles is reversed with every half-period of an oscillating flow. However, for stationary particles exposed to an oscillating flow with and without a steady velocity as shown in experimental works [3–5] and theoretical works [7], the particle velocity is zero and the relative velocity is the same as an oscillating flow. Thus the relative velocity with no particle entrainment oscillates with an amplitude of 5 m s^{-1} around a steady velocity of 10 m s^{-1} and the flow direction is always from left to right, unlike the case with particle entrainment having a flow direction reversing every half-period after a steady periodic state is reached. These results show that the heat transfer past particles with entrainment has different characteristics compared with that without entrainment.

Figure 4 shows the local Nussult number variation with angle for $Re_0 = 62.9$ and $Re_1 = 31.5$ at a frequency of 50 Hz. The local Nusselt numbers with particle entrainment are compared with the quasi-steady, local Nusselt number without particle entrainment. The Nusselt number is plotted as $Nu_\theta - 2$ to separate effects of pure conduction from convection. $Nu_\theta = 2$ corresponds to a pure conduction value. $Nu_\theta - 2$ with entrainment decreases with increasing particle velocity due to the particle entrainment (see Fig. 3), followed by the steady periodic state after about four cycles. The relative velocities with entrainment at $\tau = 0.0$, 1.0, 2.0, 3.0, 4.0 and 5.0 are 15, 6.24, 4.88, 4.64, 4.59 and 4.58 m s^{-1}, respectively, resulting in the decreasing $Nu_\theta - 2$ with decreasing relative velocity due to particle entrainment, as shown in Fig. 4. However, the relative velocity without entrainment is 15 m s^{-1}, giving $Nu_\theta - 2$ varying in the range of $0.7 \sim 10.64$, larger than $Nu_\theta - 2$ with entrainment varying in the range of $0.1 \sim 5.1$ at $\tau = 5.0$. At these dimensionless times, the flow direction at infinity is from left to right both with and without particle entrainment, in the coordinate system as shown in Fig. 1. Thus $Nu_\theta - 2$ has a maximum value at the stagnation point at $\theta = 180$ and decreases along the stream-wise direction ($\theta = 180 \rightarrow \theta = 0$). In the following dimensionless times of $\tau = 0.25$, 1.25, 2.25, 3.25, 4.25 and 5.25, the relative velocities with entrainment are 4.78, -0.095, -0.24, -1.15, -1.17 and -1.18 m s^{-1}. Thus the flow direction at $\tau = 0.25$ is from left to right with a stagnation point at $\theta = 180$. But the flow direction at $\tau = 1.25$, 2.25, 3.25, 4.25 and 5.25 is reversed to that from right to left with a stagnation point at $\theta = 0$. The relative velocity without entrainment is 10 m s^{-1} with a stagnation point at $\theta = 180$ with a flow direction from left to right, giving $Nu_\theta - 2$ varying in the range of $0.04 \sim 8.4$, larger than $Nu_\theta - 2$ with entrainment varying in the range of $-0.006 \sim 2.2$ at $\tau = 5.25$. At $\tau = 0.5$, 1.5, 2.5, 3.5, 4.5 and 5.5, the relative velocities with entrainment increases from -0.62 to -4.58 m s^{-1} with a

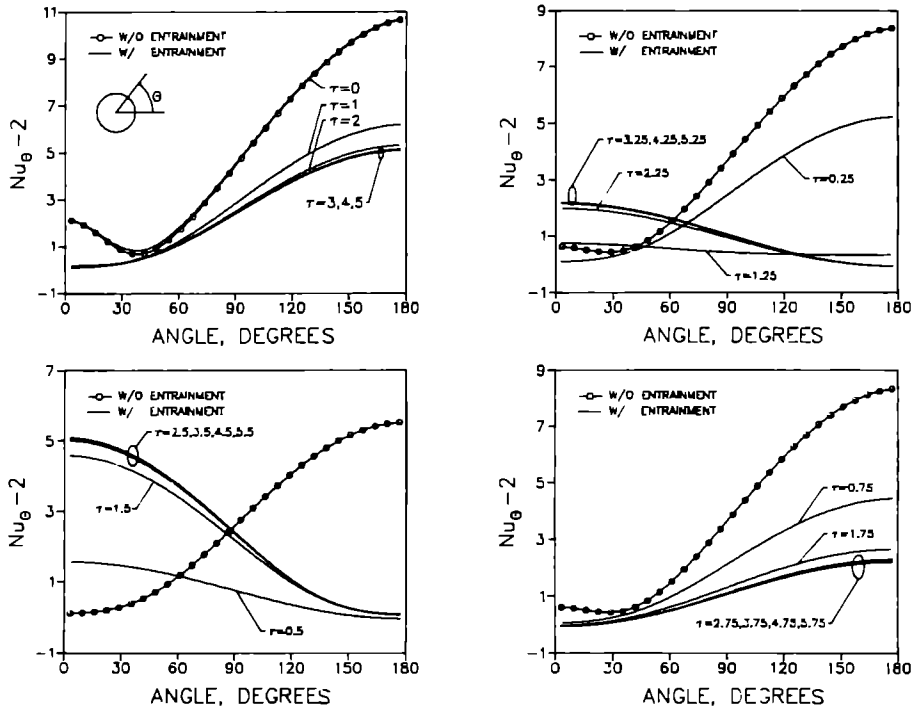

FIG. 4. Angular variation of local Nusselt number with and without particle entrainment: $Re_0 = 62.9$, $Re_1 = 31.5$, $S = 0.0005$ ($f = 50$ Hz).

flow direction from right to left. The relative velocity without entrainment is 5 m s^{-1} with a flow direction from left to right, slightly larger than -4.58 m s^{-1} with entrainment at $\tau = 5.5$. Thus $Nu_\theta - 2$ with entrainment at $\tau = 5.5$ has a symmetric profile around $\theta = 90$, compared to that without entrainment. The relative velocities at $\tau = 0.75, 1.75, 2.75, 3.75, 4.75$ and 5.75 decreases from 3.85 to 1.18 m s^{-1} with increasing particle velocity. These relative velocities with entrainment are smaller than 10 m s^{-1} without entrainment, resulting in the lower $Nu_\theta - 2$ with entrainment compared with that without entrainment.

Figure 5 shows the space-averaged Nusselt number ($Nu_s - 2$) with and without particle entrainment as a function of dimensionless time τ for the oscillating flow with steady Reynolds number $Re_0 = 62.9$ and acoustic Reynolds number $Re_1 = 31.5$ for Strouhal number of 0.001. The space-averaged Nusselt number is calculated from Nu_θ using equation (17). As shown in Fig. 5, $Nu_s - 2$ without entrainment shows the same cyclic behavior as the oscillating flow velocity U as shown in Fig. 3. However, for $Nu_s - 2$ with entrainment, another high peak at the half time of the period in each cycle is observed. This happens since the space-averaged Nusselt number is not dependent on the direction of the velocity, which changes as a result of the acoustic field, and is dependent only on the magnitude of the total flow velocity.

Figure 6 shows the oscillating flow U, the entrained particle velocity v_p and the relative velocity $(U - v_p)$ at 2000 Hz, in order to investigate the frequency effect on the heat transfer past particles entrained in an oscillating flow with a steady velocity component. Similar to the case of $f = 50$ Hz, the applied acoustic field U oscillates with an amplitude of 5 m s^{-1} around a steady velocity of 10 m s^{-1}, giving $Re_0 = 62.9$, $Re_1 = 31.5$ and $S = 0.02$. As shown in Fig. 3, it takes more than three cycles in order for the relative velocity at $f = 50$ Hz to reach a steady periodic state after the particle is almost entrained in the steady velocity U_0. Three cycles at 50 Hz corresponds to 120 cycles for 2000 Hz. Thus the results up to around 70 cycles are

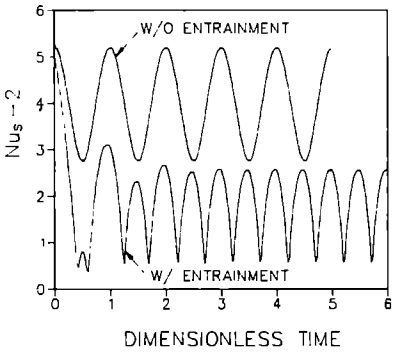

FIG. 5. Space-averaged Nusselt number with and without particle entrainment as a function of dimensionless time: $Re_0 = 62.9$, $Re_1 = 31.5$, $S = 0.0005$ ($f = 50$ Hz).

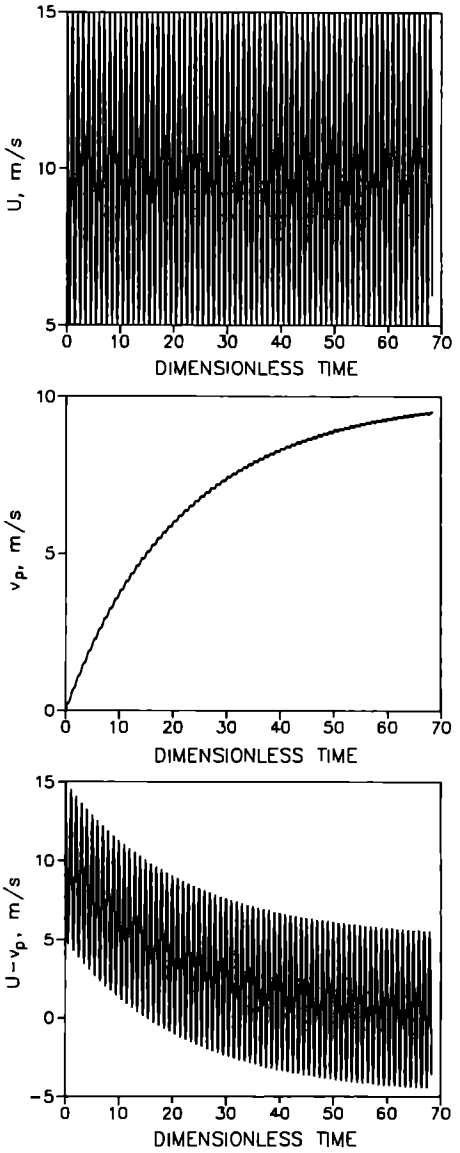

FIG. 6. Oscillating flow U, the entrained particle velocity v_p and the relative velocity $(U-v_p)$ as a function of dimensionless time: $Re_0 = 62.9$, $Re_1 = 31.5$, $S = 0.02$ ($f = 2000$ Hz).

shown in the present calculation for $f = 2000$ Hz due to severe computational time. The entrained particle velocity approaches the steady velocity U_0 ($=10$ m s^{-1}). After the initial and transient period, the relative velocity is expected to approach the oscillating flow with an amplitude of 5 m s^{-1} which is the acoustic velocity $U_1 \cos(2\pi ft)$, as shown in Fig. 6. Thus the space-averaged Nusselt number (Nu_s-2) with entrainment has different time histories compared with Nu_s-2 without entrainment, as shown in Fig. 7. Nu_s-2 without entrainment reaches a steady periodic state at an early cycle and oscillates in the range of $2.8 \sim 5.1$. However the value of Nu_s-2 with entrainment decreases during the initial and transient period until it reaches a steady periodic state. Nu_s-2 with entrainment is lower than that without entrainment due to particle entrainment.

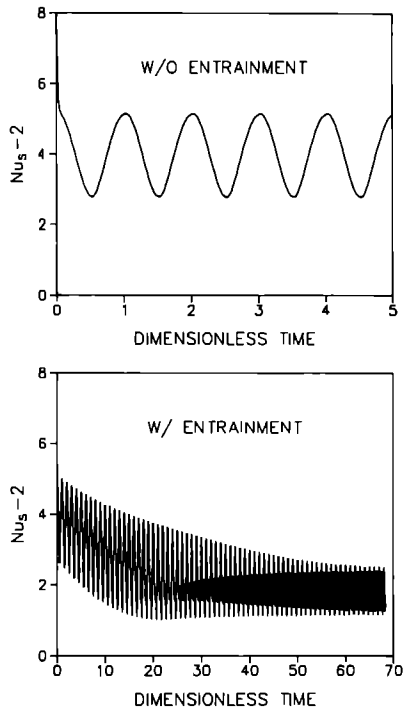

FIG. 7. Space-averaged Nusselt number with and without particle entrainment as a function of dimensionless time: $Re_0 = 62.9$, $Re_1 = 31.5$, $S = 0.02$ ($f = 2000$ Hz).

Oscillating flow without a steady velocity

Figure 8 shows the oscillating flow U, the entrained particle velocity v_p and the relative velocity $(U-v_p)$ at 50 Hz, in order to investigate heat transfer past particles entrained in an oscillating flow without a steady velocity component. The applied acoustic field U oscillates with an amplitude of 10 m s^{-1}, giving acoustic Reynolds number of 62.9 and Strouhal number of 0.0005. For this small value of the Strouhal number, the velocity and temperature field reaches a steady periodic state after an early cycle. Thus the following discussion concentrates on the results over one cycle after reaching a steady periodic state, unless it is mentioned otherwise. While the oscillating flow U oscillates with an amplitude of 10 m s^{-1}, the particle velocity v_p oscillates with an amplitude of 2.72 m s^{-1} with a phase lag of about 72° ($\tau = 0.2$). Due to this phase lag between an oscillating flow and particle velocity, the relative velocity, $U-v_p$, oscillates with an amplitude of 9.38 m s^{-1} slightly lower than an oscillating flow U which is the relative velocity without entrainment. The phase lag between an oscillating flow, U, and the relative velocity, $U-v_p$, is about 18° ($\tau = 0.05$).

Figure 9 shows the quasi-steady, local Nusselt number variation with angle without steady flow corresponding to $Re_1 = 62.9$ and $S = 0.0005$. The results with entrainment are compared with that without entrainment. At $\tau = 0.0$, the oscillating velocity is 10 m s^{-1} and the particle velocity is 1 m s^{-1}. Thus the relative velocity with entrainment is 9 m s^{-1}, lower than 10 m s^{-1} without entrainment. $Nu_\theta-2$ with

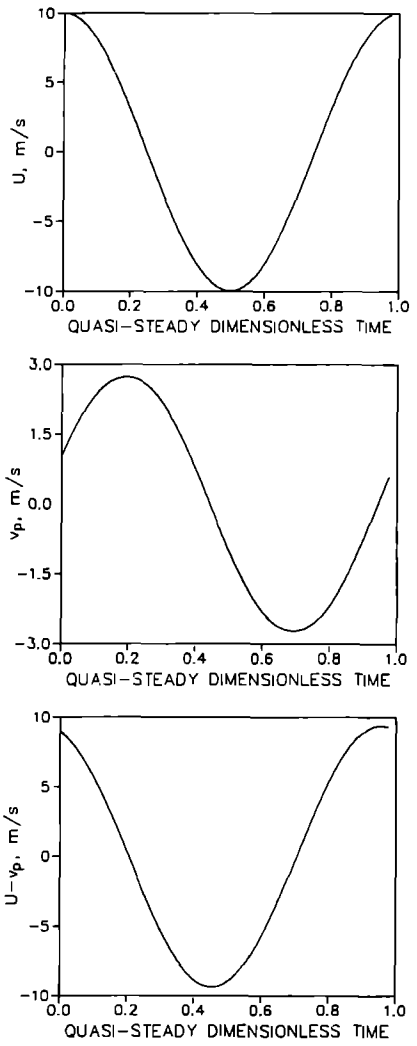

FIG. 8. Oscillating flow U, the entrained particle velocity v_p and the relative velocity $(U-v_p)$ as a function of quasi-steady dimensionless time: $Re_0 = 0$, $Re_1 = 62.9$, $S = 0.0005$ ($f = 50$ Hz).

entrainment is lower than that without entrainment, due to the difference in the relative velocity with and without entrainment. The difference in $Nu_\theta - 2$ at the stagnation point ($\theta = 180$) is about 7%. In the following dimensionless time $\tau = 0.125$, the particle velocity is 2.5 m s^{-1} for the oscillating velocity of 7.07 m s^{-1}. Thus the relative velocity with entrainment is 4.57 m s^{-1} which is 54% lower than the relative velocity without entrainment. $Nu_\theta - 2$ with entrainment at the stagnation point ($\theta = 180$) is about 25% lower than that without entrainment. At $\tau = 0.25$, the relative velocity without entrainment is 0 m s^{-1} which is the same as the oscillating velocity. As shown in refs. [20, 21], a small steady motion (acoustic streaming) is generated over a spherical particle in the presence of an acoustic field. Thus, as shown by Ha [7], it is expected that the phase lag between the applied acoustic field and the thermal boundary layer, and the steady streaming results in $Nu_\theta - 2$ without entrainment varying in the range of $0.5 \sim 0.7$, even though the relative velocity is 0 m s^{-1}. However, for the case with entrainment, the relative velocity is -2.5 m s^{-1} with a stagnation point at $\theta = 0$. Thus $Nu_\theta - 2$ with entrainment varies in the range of $-0.001 \sim 3.6$, larger than $Nu_\theta - 2$ without entrainment. In the following dimensionless time $\tau = 0.375$, the relative velocity without entrainment is -7.07 m s^{-1} which is the same magnitude as that at $\tau = 0.125$ with a flow direction from right to left. Thus $Nu_\theta - 2$ without entrainment at $\tau = 0.375$ shows a symmetric profile around $\theta = 90$, compared to $Nu_\theta - 2$ without entrainment at $\tau = 0.125$. The relative velocity with entrainment at $\tau = 0.375$ is -8.2 m s^{-1} with a flow direction from right to left. This relative velocity with entrainment at $\tau = 0.375$ m s^{-1} is about 80% larger than the relative velocity with entrainment at $\tau = 0.125$ and about 17% larger than the relative velocity without entrainment at $\tau = 0.375$. This results in the larger $Nu_\theta - 2$ with entrainment at $\tau = 0.375$, compared to that with entrainment at $\tau = 0.125$ and that without entrainment at $\tau = 0.375$. The differences in the maximum $Nu_\theta - 2$ at the stagnation point with entrainment at $\tau = 0.375$ are 8.4 and 43%, respectively, compared with that without entrainment at $\tau = 0.375$ and that with entrainment at $\tau = 0.125$. At $\tau = 0.5$, the oscillating velocity and the relative velocity without entrainment have a peak value of -10 m s^{-1}. The relative velocity with entrainment at $\tau = 0.5$ is 9 m s^{-1} which is the same magnitude as the relative velocity with entrainment at $\tau = 0.0$ and 10% lower than the relative velocity without entrainment at $\tau = 0.5$. $Nu_\theta - 2$ with entrainment at $\tau = 0.5$ has a symmetric shape around $\theta = 90$, compared with $Nu_\theta - 2$ with entrainment at $\tau = 0$, and is lower than $Nu_\theta - 2$ without entrainment at $\tau = 0.5$ with 7.5% difference at a stagnation point. The distribution of $Nu_\theta - 2$ with and without particle entrainment at a dimensionless time from $\tau = 0.5$ to 1.0 is very similar to that from $\tau = 0.0$ to 0.5 except that they are anti-symmetric.

The space-averaged Nusselt number with and without particle entrainment is shown in Fig. 10 for $Re_1 = 62.9$ and $Re_0 = 0.0$ for $S = 0.0005$ ($f = 50$ Hz) as a function of dimensionless time. $Nu_s - 2$ with and without entrainment has two high and low peak values over one cycle corresponding to the maximum and minimum values of the relative velocity with and without entrainment, respectively. $Nu_s - 2$ with entrainment varies in the range of $0.68 \sim 3.84$ over one cycle after the steady periodic state has been reached, whereas $Nu_s - 2$ without entrainment is in the range of $0.65 \sim 4.04$, due to about 6% difference in the relative velocity with and without entrainment. The phase lag between the space-averaged Nusselt number with and without entrainment is about 18°.

Figure 11 shows the oscillating flow U, the entrained particle velocity v_p and the relative velocity

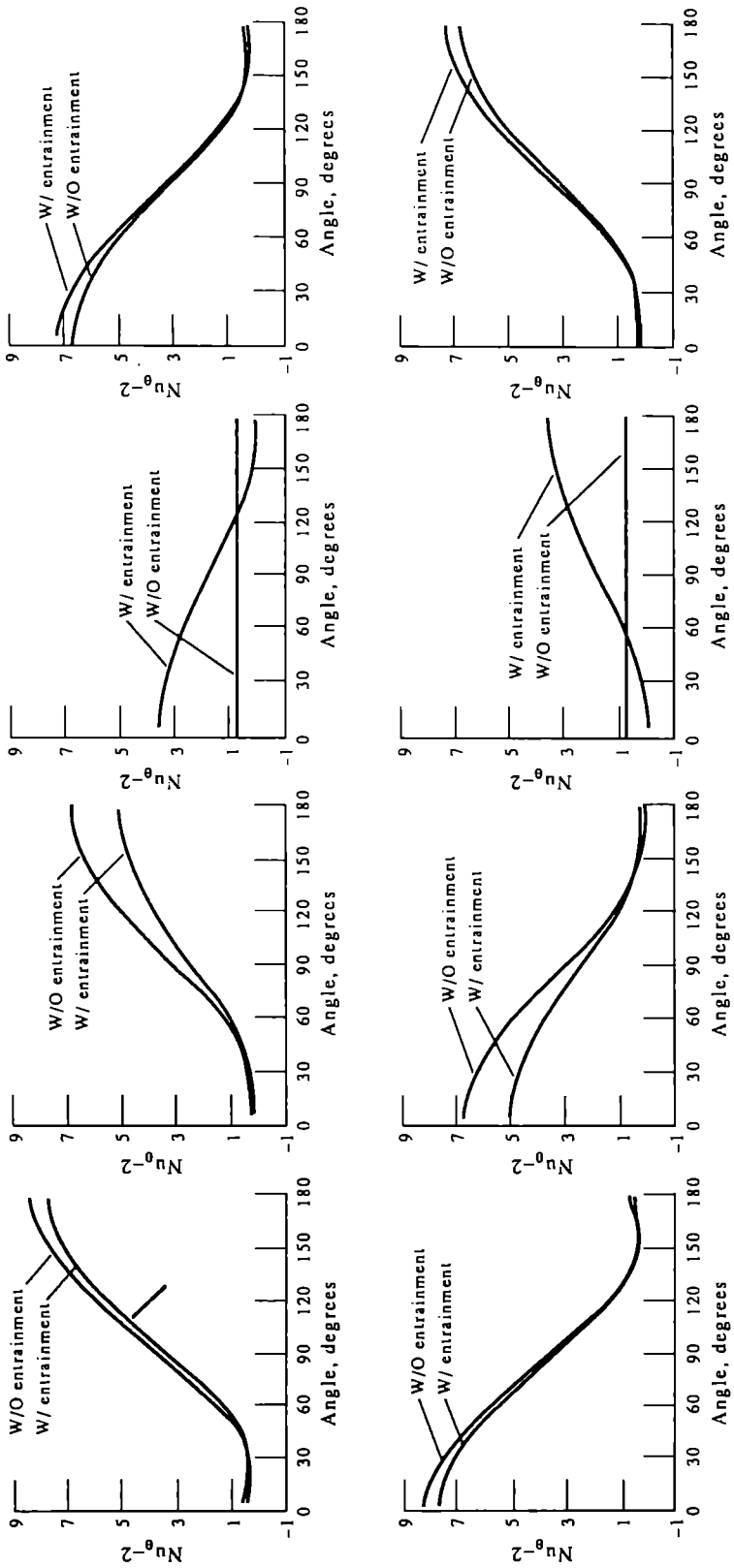

FIG. 9. Angular variation of local Nusselt number with and without particle entrainment: $Re_0 = 0$, $Re_1 = 62.9$, $S = 0.0005$ ($f = 50$ Hz).

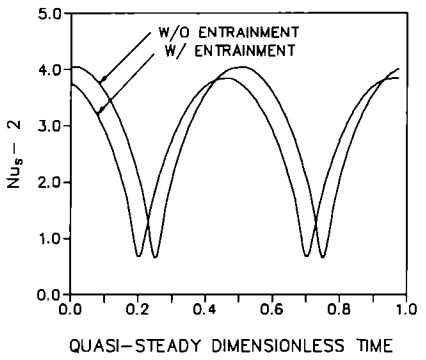

FIG. 10. Space-averaged Nusselt number with and without particle entrainment as a function of quasi-steady dimensionless time: $Re_0 = 0$, $Re_1 = 62.9$, $S = 0.0005$ ($f = 50$ Hz).

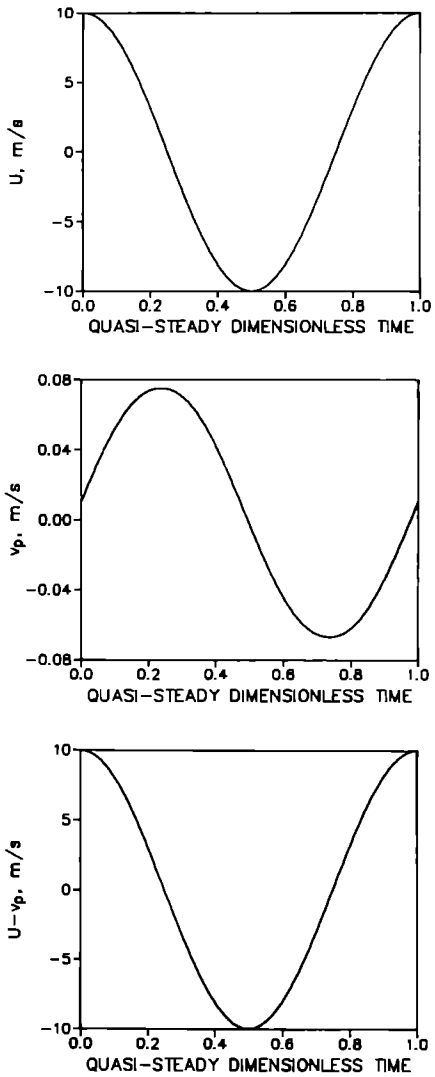

FIG. 11. Oscillating flow U, the entrained particle velocity v_p and the relative velocity $(U - v_p)$ as a function of quasi-steady dimensionless time: $Re_0 = 0$, $Re_1 = 62.9$, $S = 0.02$ ($f = 2000$ Hz).

$(U - v_p)$ for $Re_1 = 62.9$ and $S = 0.02$ ($f = 2000$ Hz). The particle velocity oscillates with an amplitude of about 0.07 m s^{-1} with 81° phase lag ($\tau = 0.225$) between U and v_p. Since the particle velocity with particle entrainment oscillates with very small amplitude, the relative velocity with entrainment is almost the same as the oscillating flow velocity U which is the relative velocity without entrainment. Thus the local and space-averaged Nusselt number with particle entrainment is almost the same as that without particle entrainment. Since the results for the local and space-averaged Nusselt number without particle entrainment $f = 2000$ Hz has been shown in detail by Ha [7], the discussion about these results are not shown in the present paper.

SUMMARY AND CONCLUSIONS

The axisymmetric and laminar conservation equations for mass, momentum and energy are solved numerically in order to investigate the heat transfer past a single spherical particle entrained in an oscillating flow with and without a steady velocity component. The results with particle entrainment are compared with the case without particle entrainment. The following are the major findings of the present studies.

The moving particle in the presence of an oscillating flow with a steady velocity is entrained in the steady velocity U_0 and the relative velocity close to the oscillating velocity $U_1 \cos(2\pi f t)$ can be used for heat transfer past particles. However, for the stationary particles fixed in the atmosphere, the sum of oscillating and steady velocity is used for heat transfer past particles. This results in the lower space-averaged Nusselt number with particle entrainment compared with that without particle entrainment, corresponding to almost the steady velocity.

In the case of an oscillating flow without a steady velocity, with increasing frequency, the magnitude of particle entrainment decreases and the phase lag between the moving particle and the oscillating flow increases. At 50 Hz, even though the particle is entrained substantially in the oscillating flow, the relative velocity between the flow and the particle has an amplitude slightly lower than that of oscillating flow U due to the phase lag existing between the moving particle and the oscillating flow. This results in the slightly lower space-averaged Nusselt number with entrainment compared with the case without entrainment. The difference in the maximum value of $Nu_s - 2$ with and without particle entrainment is about 5.2% for $Re_0 = 0$, $Re_1 = 62.9$ and $S = 0.0005$ ($f = 50$ Hz) and the phase lag between $Nu_s - 2$ with and without entrainment is about 18°. If the frequency is increased to 2000 Hz, the particle entrainment is very small and the relative velocity with and without particle entrainment is almost the same, resulting in almost the same space-averaged Nusselt number with and without particle entrainment.

REFERENCES

1. R. C. Marthelli and L. M. K. Boelter, The effect of vibration on heat transfer by free convection from a horizontal cylinder, *Proc. 5th Int. Congress of Applied Mechanics*, pp. 578–584 (1939).
2. C. B. Baxi and A. Ramachandran, Effect of vibration on heat transfer from spheres, *Trans. ASME, J. Heat Transfer* 337–344 (1969).
3. Y. Mori, M. Imabayashi, K. Hijikata and Y. Yoshida, Unsteady heat and mass transfer from spheres, *Int. J. Heat Mass Transfer* **12**, 571–585 (1969).
4. H. Gibert and H. Angelino, Transferts de matiere entre une sphere soumise a des vibrations et un liquide en mouvement, *Int. J. Heat Mass Transfer* **17**, 625–632 (1974).
5. P. S. Larsen and J. W. Jensen, Evaporation rates of drops in forced convection with superposed transverse sound field, *Int. J. Heat Mass Transfer* **21**, 511–517 (1978).
6. S. A. Rawson, An experimental investigation of the influence of high intensity acoustics on heat and mass transfer rates from spheres as related to coal–water slurry fuel combustion enhancement, M.S. Thesis, Pennsylvania State University (1988).
7. M. Y. Ha, A theoretical study of augmentation of particle combustion via acoustic enhancement of heat and mass transfer, Ph.D. Thesis, Pennsylvania State University (1990).
8. B. T. Zinn, J. R. Carvalho, Jr., N. Miller and B. R. Daniel, Pulsating combustion of coal in a Rijke type combustor, *19th Symp. (Int.) on Combustion*, The Combustion Institute, pp. 1197–1203 (1982).
9. R. J. Faeser, Acoustic enhancement of pulverized coal combustion, ASME Paper, 84-WA/NCA-18 (1984).
10. G. M. Koopmann, A. W. Scaroni, S. Yavuzkurt, G. Reethof, P. Ramachandran and M. Y. Ha, Acoustically enhanced combustion of micronized coal water slurry fuel, Final Report to DOE/METC under Contract No. DE-RA21-86MC23257 (1989).
11. S. Yavuzkurt, M. Y. Ha, G. M. Koopmann and A. W. Scaroni, A model of the enhancement of coal combustion using high intensity acoustic fields, *1989 Natn. Heat Transfer Conf.*, HTD-Vol. 106, *Heat Transfer Phenomena in Radiation, Combustion and Fires*, Philadelphia, pp. 439–446, 6–9 August (1989).
12. S. Yavuzkurt, M. Y. Ha, G. M. Koopmann and A. W. Scaroni, A model of the enhancement of the combustion of coal water slurry fuels using high intensity acoustic fields, 89-WA/NCA-2, ASME Winter Annual Meeting, San Francisco, 10–15 December (1989).
13. S. V. Patankar, *Numerical Heat Transfer and Fluid Flow*, Hemisphere, Washington, DC (1980).
14. J. P. Van Doormaal and G. D. Raithby, Enhancement of the SIMPLE method for predicting incompressible fluid flow, *Numer. Heat Transfer* **7**, 147–163 (1982).
15. R. Clift, J. R. Grace and M. E. Weber, *Bubbles, Drops, and Particles*, Academic Press, New York (1978).
16. N. N. Sayegh and W. H. Gauvin, Numerical analysis of variable property heat transfer to a single sphere in high temperature surroundings, *A.I.Ch.E. Jl* **25**(3), 522–534 (1979).
17. T. Yuge, Experiments on heat transfer from spheres including combined natural and forced convection, *J. Heat Transfer, Trans. ASME, Series C* **82**, 214–220 (1960).
18. K. Wong, S. Lee and C. Chen, Finite element solution of laminar combined convection from a sphere, *J. Heat Transfer* **108**, 860–865 (1986).
19. W. E. Ranz and W. R. Marshall, Evaporation from drops, *Chem. Engng Prog.* **48**, 141–146, 173–180 (1952).
20. J. M. Andres and U. Ingard, Acoustic streaming at high Reynolds number, *J. Acoust. Soc. Am.* **25**(5), 928–932 (September 1953).
21. J. M. Andres and U. Ingard, Acoustic streaming at low Reynolds number, *J. Acoust. Soc. Am.* **25**(5), 932–938 (September 1953).